Science Advances
AAAS

advances.sciencemag.org/cgi/content/full/6/4/eaax2642/DC1

Supplementary Materials for

Animal simulations facilitate smart drug design through prediction of nanomaterial transport to individual tissue cells

Edward Price and Andre J. Gesquiere*

*Corresponding author. Email: andre@ucf.edu

Published 22 January 2020, *Sci. Adv.* **6**, eaax2642 (2020)
DOI: 10.1126/sciadv.aax2642

This PDF file includes:

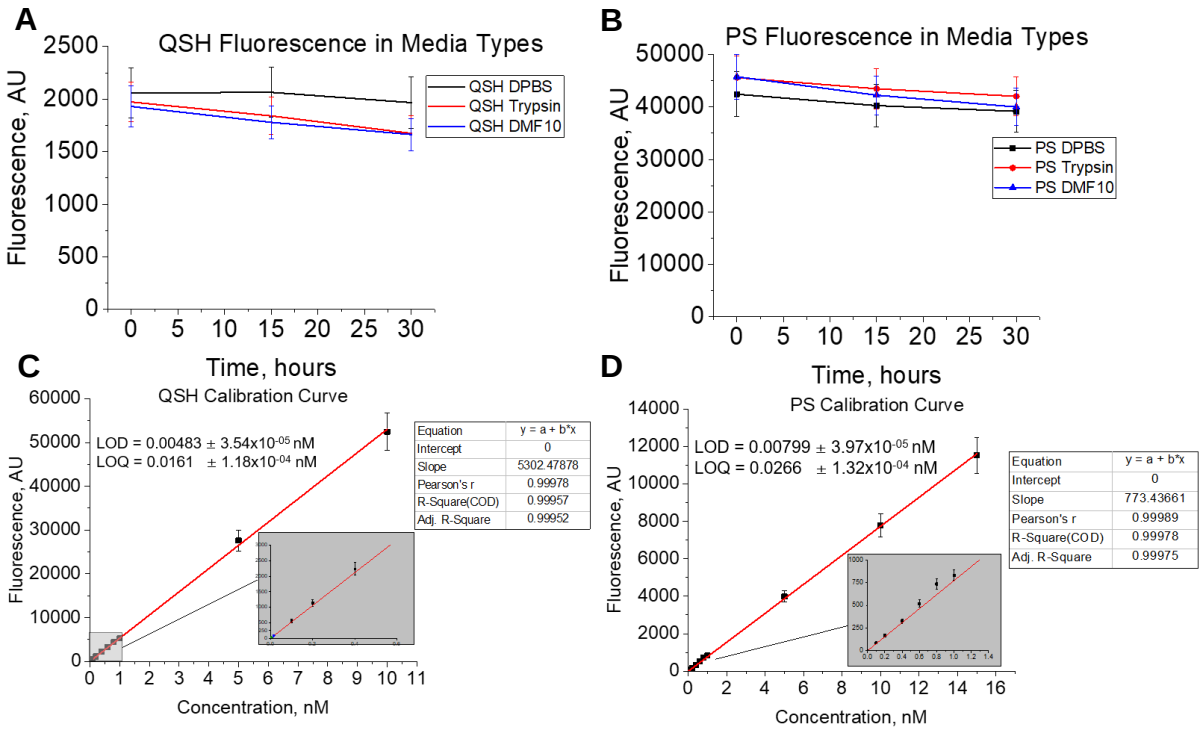

Fig. S1. Quality assurance on fluorescence signal obtained from NMs in biological solutions. (**A** and **B**) Fluorescence signal for prolonged periods of time under exposure to complete growth media (DMF10), DPBS, and trypsin for (A) QSH and (B) PS. (**C** and **D**) Calibration curves used to determine the limits of detection (LOD) and quantiation (LOQ) for (C) QSH and (D) PS.

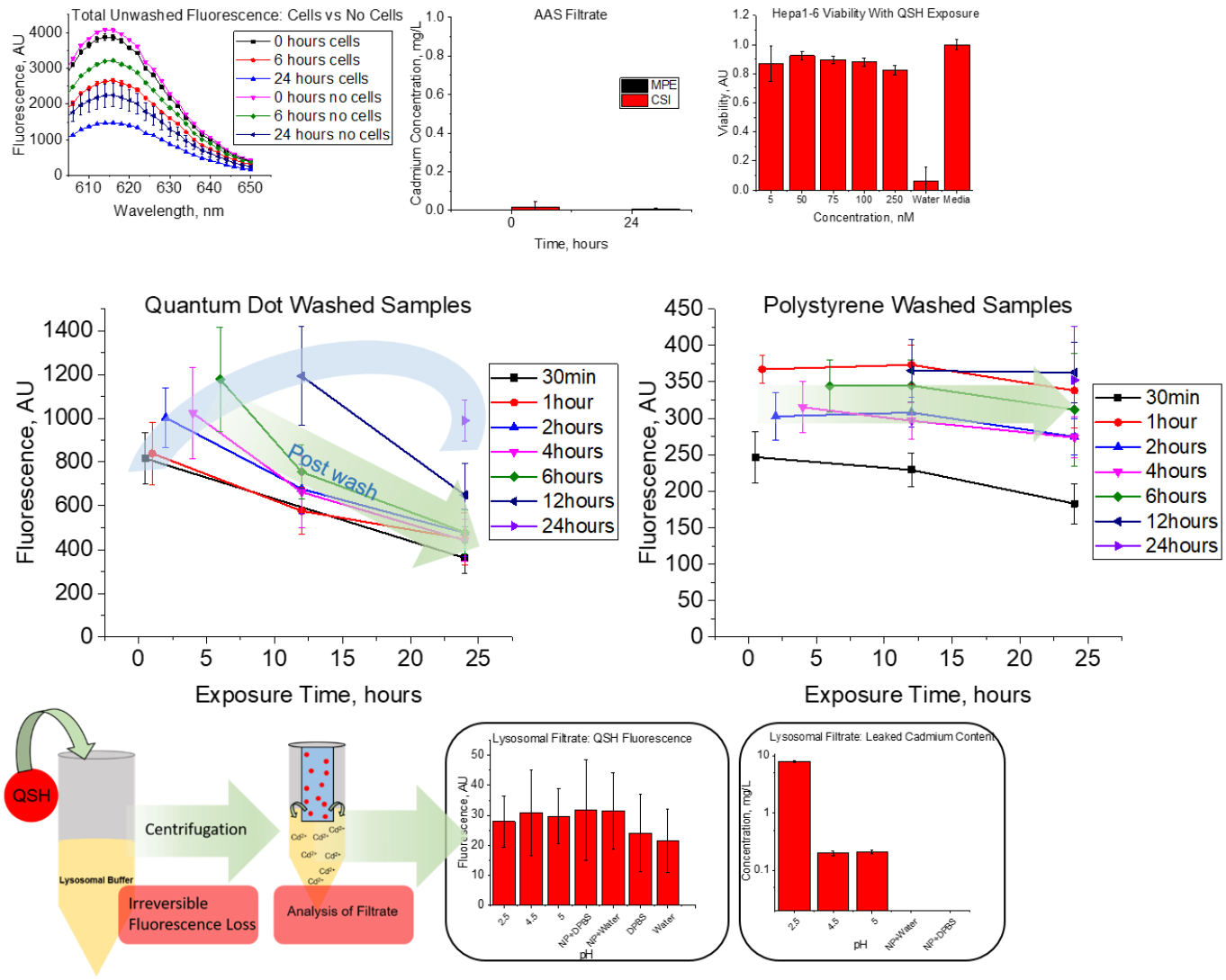

Fig. S2. Cellular and lysosomal degradation studies supporting evidence of cellular-induced degradation on fluorescence in kinetic assay.

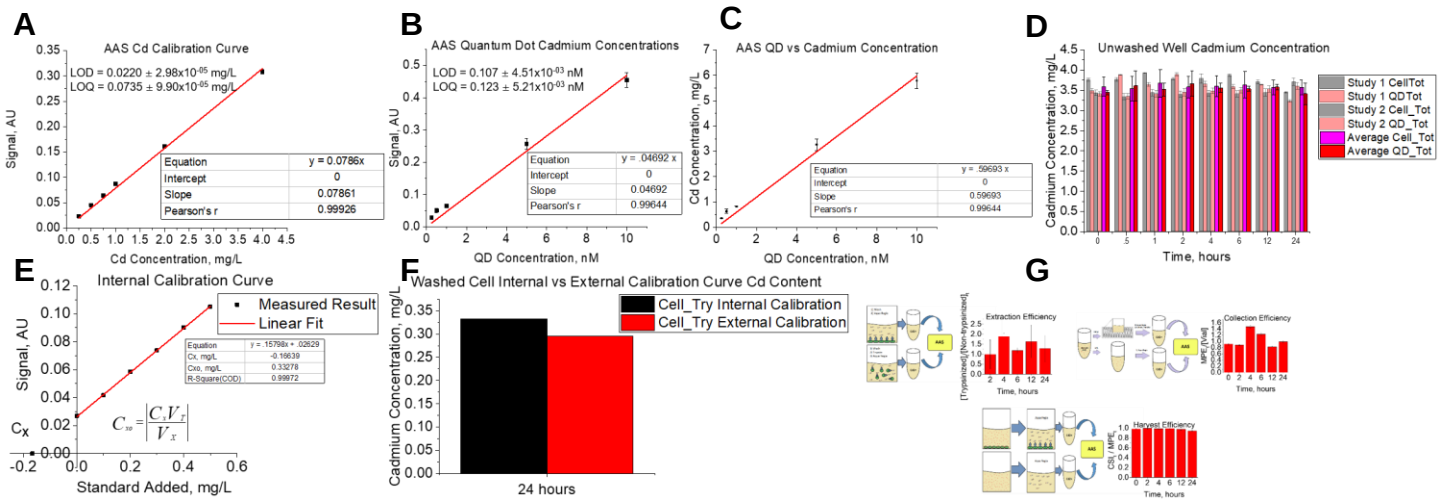

Fig. S3. Validation of QSH data by AAS. (**A**-**C**) Calibration curves for (A) $Cd(NO_3)_2$ and (B) QSH with their respective limits of detection (LOD) and quantitation (LOQ) that were used for determining the (C) calibration curve correlating cadmium concentrations (mg/L) to QD concentrations (nM).(**D**) Cadmium concentrations for unwashed wells containing cells (CSI_t) and no cells (MPE_t) as a basis for assuring cadmium content remains constant. (**E** and **F**) Method of standard addition (E) and external calibration were compared to determine if total uptake differed at 24 hours (F).(**G**) Extraction, harvest, and collection efficiencies to determine if all cadmium was extracted from cell interior, harvested from wells, and collected from entire well.

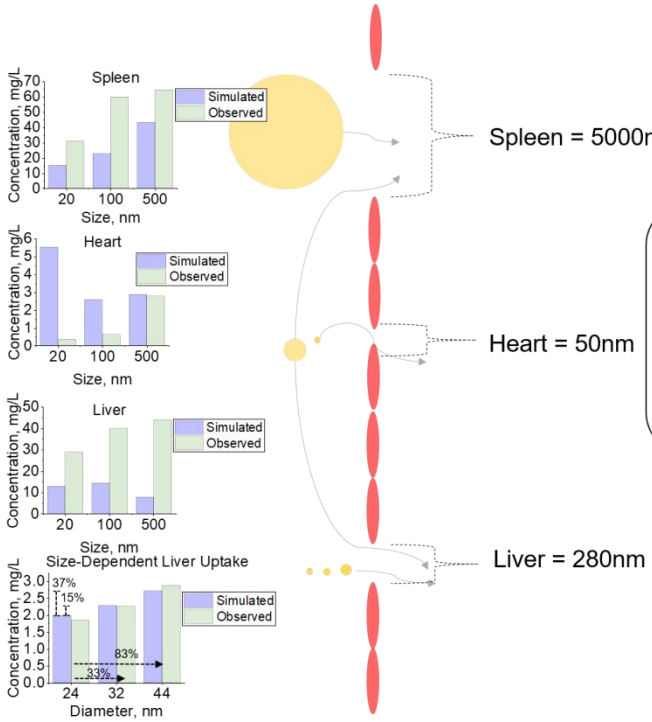

Tissue	Pore Diameter (nm)	Cited Species	Source	Type	Region
Liver	280	Rodent	Sarin et al. 2010	Sinusoidal	N/A
Kidney	200	Rat	Fujita et al. 1976	Fenestrated	Kidney glomerulus
Spleen	5000	Dog	Sarin et al. 2010	Sinusoidal	Splenic red pulp
Muscle	80	Rat	Korneliussen et al. 1975	Continuous, Fenestrated	Skeletal muscle
Heart	50	Multiple	Weihe and Kambach 1978	Fenestrated	AV-node and AV-bundle
Small Int	80	Rat	Simionescu et al. 1974	Fenestrated	Jejenum
Bone	40000	Mouse	Okada et al. 2017	Sinusoidal	Marrow
Skin	60	Rat	Imayama 1981	Fenestrated	Sole skin
Brain	0.99	Rat	Sarin et al. 2010	Non-Fenestrated	Brain-Spinal Cord, Inter-endothelial junction
Large Int	80	Rat	Sarin et al. 2010	Fenestrated	N/A
Lung	27	Pig	Townsley et al. 2013	Fenestrated	N/A

**Multiple indicates Rat, Rabbit, Cat, NHP, Mouse*
**N/A indicates region was not explicitely stated*

Fig. S4. Cellular analysis of NM uptake in varying tissues for NM with different diameters. Cellular uptake of NMs with diameters of 20, 100, and 500nm for spleen, heart, and liver with fenestrae diameters of 5000, 50, and 280nm respectively. Sensitivity analysis of incremental changes in NM diameter (24, 32, and 44nm) with subsequent liver cell uptake were performed. All simulated (predicted) outputs are compared to observed data from literature cellular datasets. Table includes reflection coefficients taken from various literature sources for different species (*71-77*).

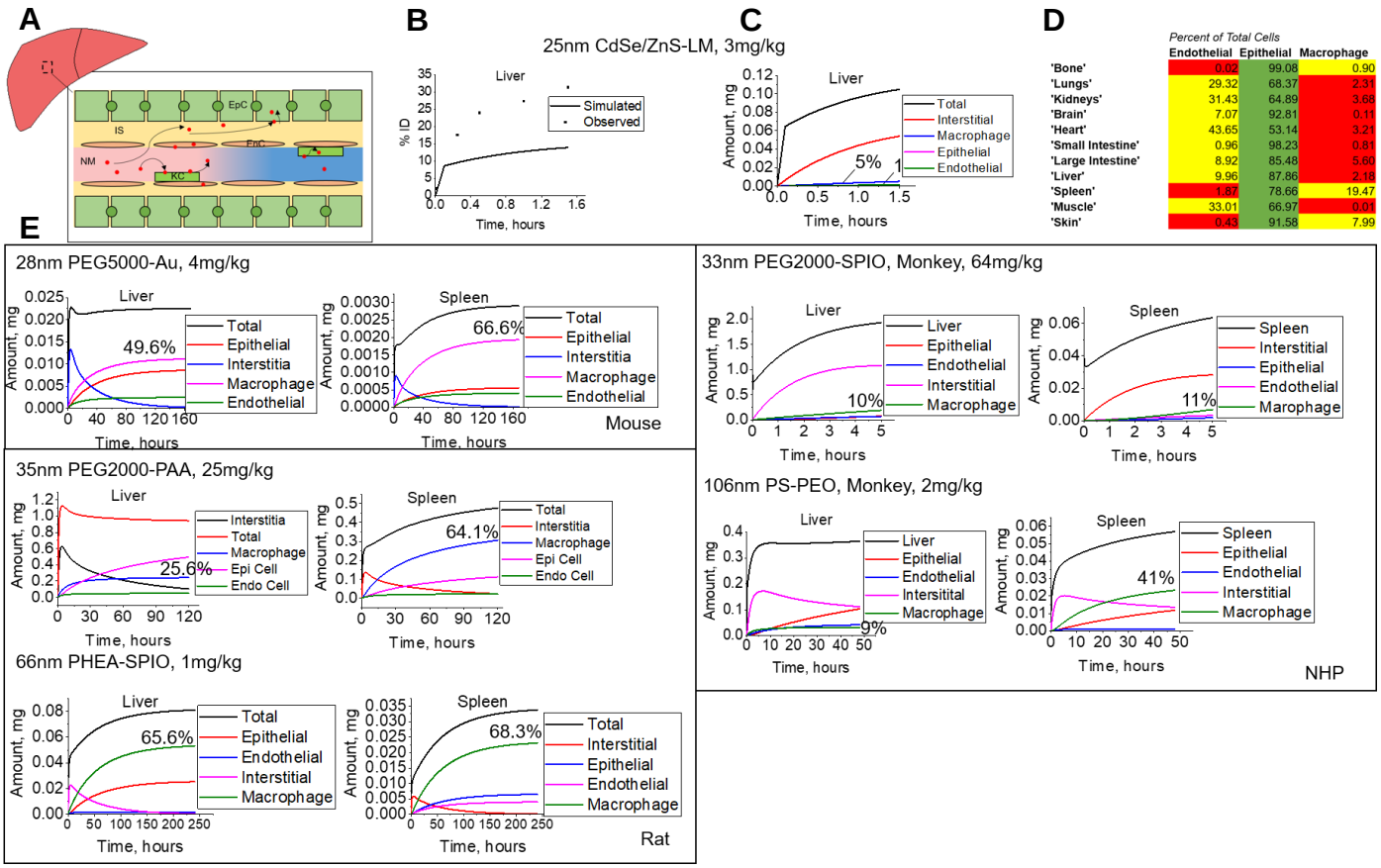

Fig. S5. Liver and spleen total and cellular uptake of NM for multiple species and NM types. (**A**) Schematic of liver cellular composition which consists of endothelial (EnC), epithelial (EpC), and macrophage (KC) cellular content. The NM from the vasculature must travel through the EnC fenestrae to reach the interstitial space (IS). (**B** and **C**) Total liver uptake (B) and cellular content (C) in rat liver tissue. (**D**) All tissue cellular content for tissues used in this study. (**E**) NM uptake in spleen and liver epithelial and endothelial cells, macrophages, and interstitia for Mouse, NHP, and Rats.

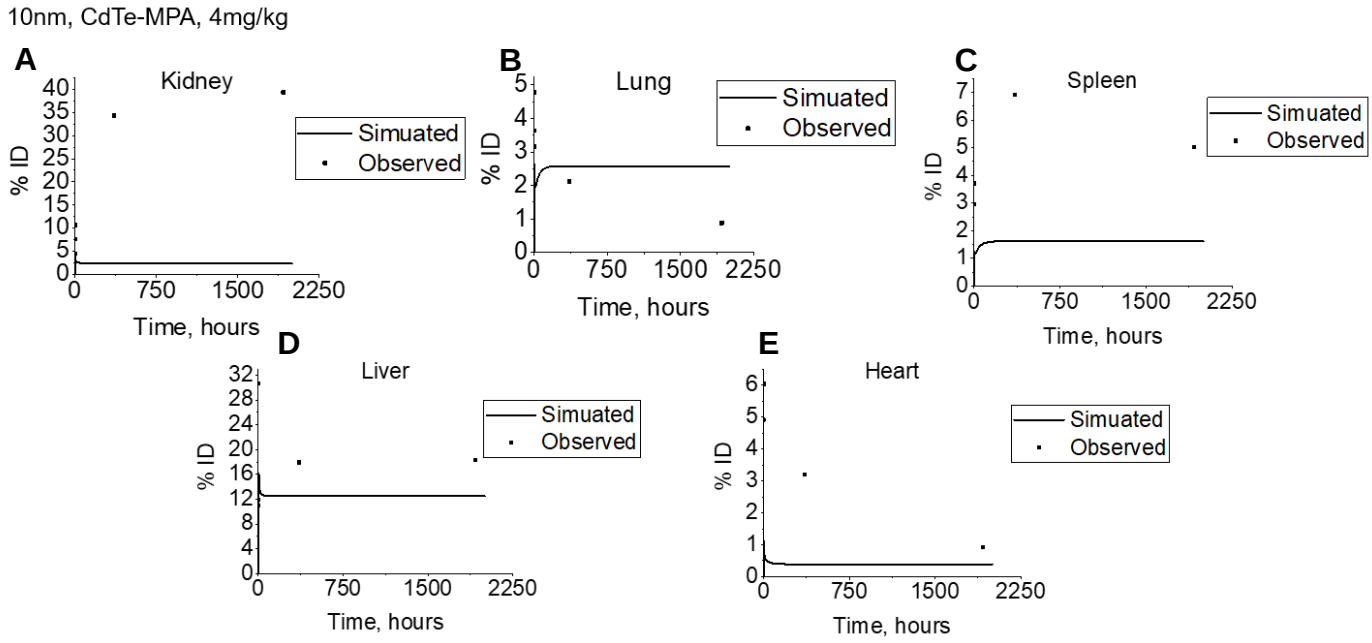

Fig. S6. Total tissue content for mouse intravenous dosing studies. (**A**-**E**) Total percent of intravenous dose predicted by our group and reported in published live animal studies for (A) Kidney, (B), Lungs, (C) Spleen, (D) Liver, and (E) Heart tissue.

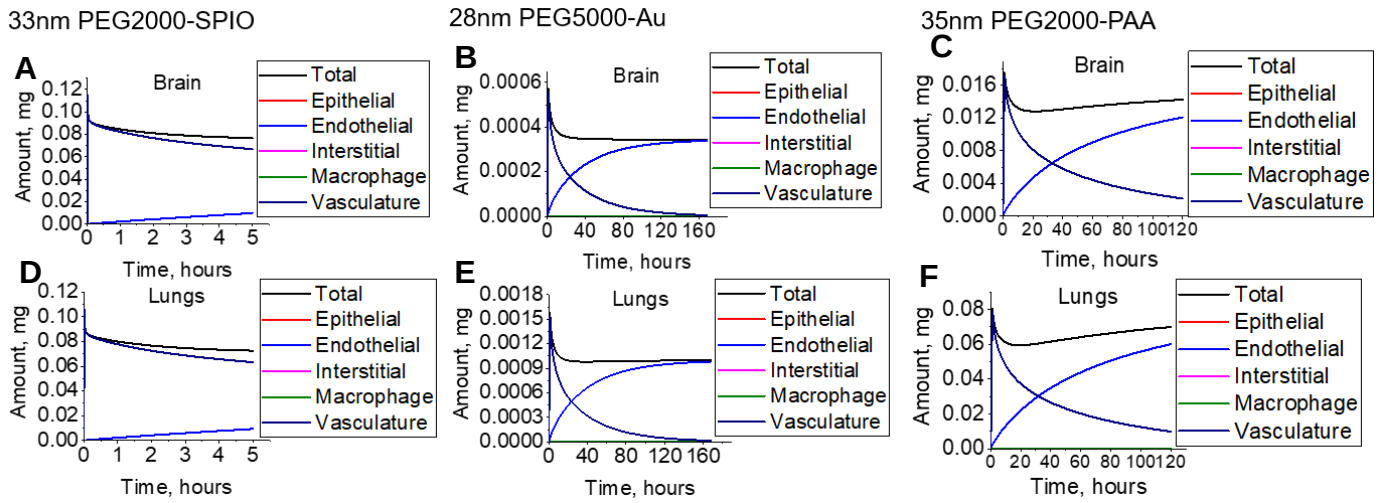

Fig. S7. Brain and lung NM subtissue content. (**A**-**C**) Brain sub-tissue content for (A) 33nm PEG2000-SPIO, (B) 28nm PEG5000-Au, and (C) 35nm PEG2000-PAA. (**D**-**F**) Lung sub-tissue content for (D) 33nm PEG200-SPIO, (E) 28nm PEG5000-Au, and (F) 35nm PEG2000-PAA.

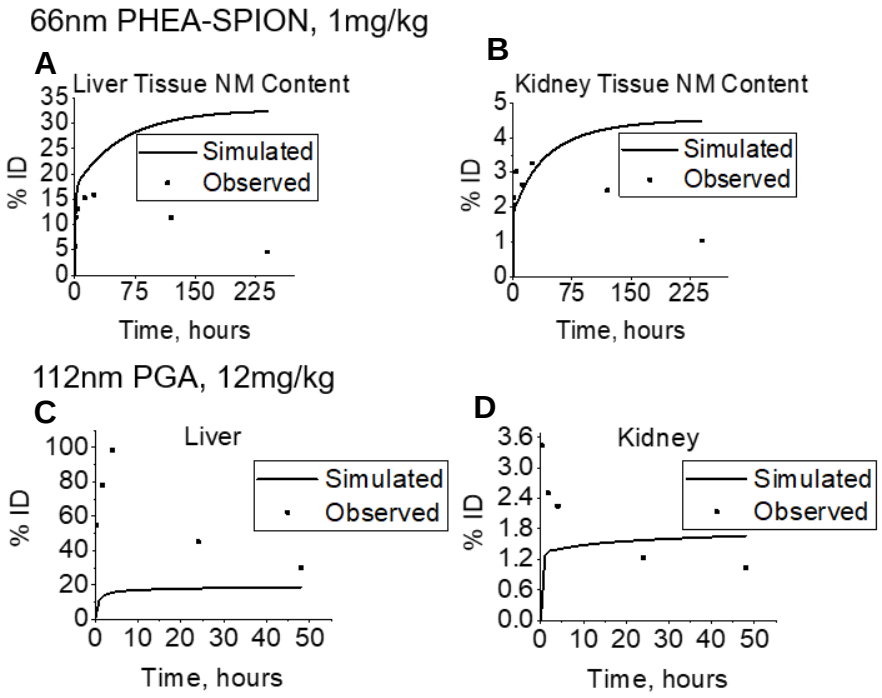

Fig. S8. Analysis of tissues involved in NM metabolism. (**A**-**D**) Liver and Kidney tissue uptake for (A, B) Heavily metabolized 66nm PHEA-SPION and (C, D) Minimally metabolized112nm PGA NM.

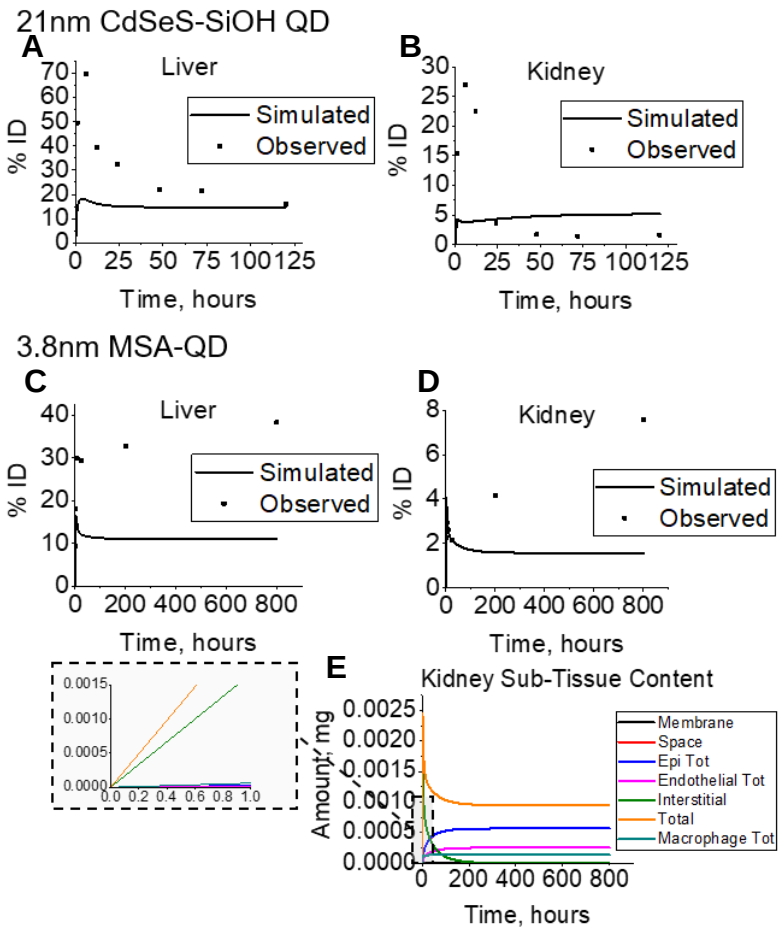

Fig. S9. Liver and kidney total NM content for 21- and 3.8-nm-sized QDs. (**A**-**D**) Total tissue level NM content for liver and kidney for (A, B) 21nm CdSeS-SiOH QD and (C, D) 3.8nm MSA-QD. (**E**) Cellular and interstitial analysis of the smaller, 3.8nm-sized QD inside kidney tissue.

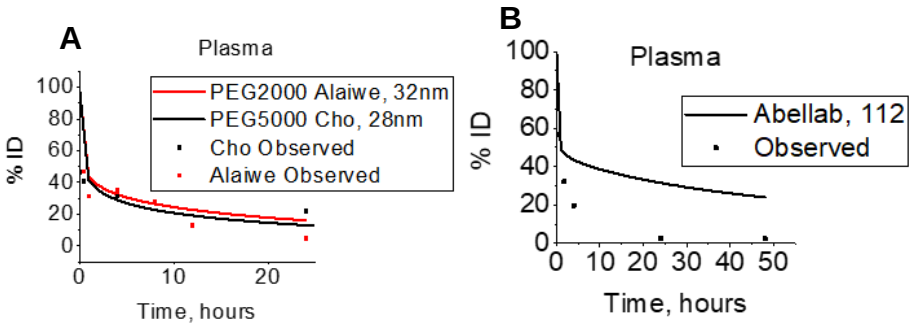

Fig. S10. Plasma NM content and correlation with PEG chain length. (**A**) Plasma uptake data for NMs of varying PEG chain lengths. (**B**) Plasma uptake data for NM exhibiting substantial excretion profile.